

[Supporting Information](#)

Field-induced slow magnetic relaxation behaviours in binuclear cobalt(II) metallocycle and exchange-coupled cluster

Dong Shao,*^{a,e} Shruti Moorthy, ^c Yue Zhou, ^a Si-Tong Wu, ^a Jing-Yan Zhu, ^a Jiong Yang, ^d Dong-Qing Wu, *^b Zhengfang Tian, ^a Saurabh Kumar Singh *^c

^a Hubei Key Laboratory of Processing and Application of Catalytic Materials, College of Chemistry and Chemical Engineering, Huanggang Normal University, Huanggang 438000, P. R. China.

^b Engineering Research Center of Photoelectric Functional Material, School of Chemistry and Chemical Engineering, Shangqiu Normal University, Shangqiu 476000, P. R. China

^c Department of Chemistry, Indian Institute of Technology Hyderabad, Kandi-502285, Sangareddy, Telangana, India.

^d Department of Chemistry, Southern University of Science and Technology, Shenzhen 518055, P. R. China

^e State Key Laboratory of Coordination Chemistry, Nanjing University, Nanjing, 210023, China

Correspondence and requests for materials should be addressed to

E-mail: shaodong@nju.edu.cn or sksingh@chy.iith.ac.in

Table of Content

Experimental Section.....	4
Computation Methodology.....	5
Figure S1. Comparison of the experimental PXRD patterns of 1 (a) and 2 (b) with the simulated patterns from their single crystal structures based on bulk sample. (c) Comparison of the experimental PXRD patterns of 2 with the simulated pattern based on the well-grounded hand-picked single crystals sample.	7
Figure S2. Crystal structure of the impurity in bulk sample of 2	8
Figure S3. Thermogravimetric curves of 1 and 2 measured under the nitrogen atmosphere upon the continuous heating with the $10\text{ }^{\circ}\text{C}\cdot\text{min}^{-1}$ rate.	9
Figure S4. The designed cobalt dimer complex with tetrahedral Co^{2+} centers.....	10
Figure S5. The asymmetric units of 1 and 2	11
Table S1. Selected bond lengths (\AA) and angles [$^{\circ}$] for 1	12
Table S2. Selected bond lengths (\AA) and angles [$^{\circ}$] for 2	13
Table S3. Continuous Shape Measure (CSM) analysis for Co(II) ions in 1 and 2	14
Figure S6. Packing diagram of the discrete Co_2 metallocycle of 1 along crystallographic b axis.	15
Figure S7. Variable-temperature magnetic susceptibility for 2 measured under applied dc field of 0.1 T	16
Figure S8. Frequency dependence of the in-phase (χ') and out-of-phase (χ'') ac susceptibilities measured under zero dc field at 2.0 K for 1 and 2	17
Figure S9. Temperature dependence of the in-phase (χ') and out-of-phase (χ'') part of the ac susceptibilities measured under 1 kOe dc field for 1 and 2	18
Figure S10. Cole-cole plot for 1 and 2 under 1000 Oe dc field. The solid lines are the best fits to the experiments with the generalized Debye model.	19
Table S4. Relaxation fitting parameters from the least-square fitting of the Cole-Cole plots of 1 according to the generalized Debye model.....	20
Table S5. Relaxation fitting parameters from the least-square fitting of the Cole-Cole plots of 2 according to the generalized Debye model.....	20
Table S6. CASSCF/NEVPT2 computed 10 spin-free quartets (red) and 40 spin-free doublets (blue) states along with the spin-orbit states for 1 . All the values are reported here in cm^{-1}	21
Table S7. CASSCF/NEVPT2 computed 10 spin-free quartets (red) and 40 spin-free doublet (blue) states along with the spin-orbit states for complex 2 . All the values are reported here in cm^{-1} ..	23
Table S8. CASSCF (7,5)+NEVPT2 computed Spin-Hamiltonian parameter (g , D , $ E/D $) along with wave function decomposition analysis for complexes 1 and 2 . All these data obtained from ORCA code.	26
Figure S11. NEVPT2 computed orientation of computed effective g-tensor and D-tensor for complex 1 . Color code: Co(cyan), N (blue), S(yellow), C (grey), O(red). The hydrogens are omitted for clarity.	28

Figure S12. NEVPT2 computed orientation of computed effective g-tensor and D-tensor for complex 2. Color code: Co(cyan), N (blue), S(yellow), C (grey), O(red). The hydrogens are omitted for clarity.	29
Figure S13. Model complex prepared to study the variation in spin-Hamiltonian parameters with change in \angle N-Co-N. Color code: Co (cyan); N (blue), O (red), S (yellow), C (grey).....	30
Table S9. NEVPT2 computed variation of the spin-Hamiltonian parameters (D and E/D) with change in \angle N-Co-N for model complex 2.	31
Figure S14. NEVPT2 computed variation of energy of the first three excited states (in cm^{-1}) with change in the \angle N-Co-N ($^{\circ}$) for model complex 2 (black line: ground state; red, green, blue: first, second and third excited states respectively)	32
Table S10. Energies (in cm^{-1}) of spin-free ground and first excited state of the $S = 3/2$ states spanned by the d^7 configuration in 1 and 2, and the constituting electronic configurations.	33
Table S11. Energies (in cm^{-1}) of spin-free of the ground and the first excited states of the $S = 3/2$ states spanned by the d^7 configuration in magneto-structural correlation developed for complex 2, and the constituting electronic configurations.....	34
Table S12. AILFT computed d-orbital ordering in the magneto-structural correlation developed for complex 2.	38
Table S13. AILFT derived ligand field parameters computed at CASSCF (in parentheses) and NEVPT2 level of theory for complexes 1 and 2. The values of B , C , ξ parameters are provided in units of cm^{-1}	39
Figure S15. POLY_ANISO simulated energy spectrum of exchange coupled states in complex 1. Black bars are the energies of exchange-coupled states arranged according to the associated magnetic moments. The dotted red lines and numbers represent the possibility of quantum tunnelling between the states, while blue arrows/numbers represent the possibility of Orbach relaxations.	40
Table S14. BS-DFT computed energies of high-spin and broken-symmetry solution of complex 1 using $H=-2JS_1S_2$ formalism.....	41
Table S15. BS-DFT computed energies of high-spin and broken-symmetry solution of complex 2 using $H=-2JS_1S_2$ formalism.....	42
Table S16. Energies of low-lying pseudo-KDs, associated g-values, and tunneling splitting for complex 1 obtained from the POLY_ANISO simulation.	43
Table S17. RASSCF computed D , g , and E values for complexes 1 and 2 obtained from MOLCAS code.	44
Figure S16. DFT calculated spin-density plot for the ground state (S=0) of complex (a) 1 and (b) 2; the positive and negative spin densities are represented by orange and blue colour, respectively. The isodensity surface represented here corresponds to a value of $0.002 \text{ e}^-/\text{bohr}^3$	45
Figure S17. DFT calculated overlap integrals for complex (a) 1 and (b) 2. The isodensity surface represented here corresponds to a value of $0.03 \text{ e}^-/\text{bohr}^3$	46
Reference:.....	47

Experimental Section

General Procedure. Powder X-ray diffraction data (PXRD) were recorded at room temperature on a Bruker D8 Advance diffractometers with Cu K α X-ray source ($\lambda = 1.54056 \text{ \AA}$) operated at 40 kV and 40 mA. Infrared (IR) spectra data were measured on KBr pellets using a Nexus 870 FT-IR spectrometer in the range of 4000-400 cm $^{-1}$. Elemental analyses of C, H, and N were performed at an Elementar Vario MICRO analyzer. Thermal gravimetric analysis (TGA) was measured in Al₂O₃ crucibles using a PerkinElmer Thermal Analysis in the temperature range of 30-800 °C under flowing argon at a heating rate of 10 °C/min.

Magnetic Measurements. Magnetic susceptibility measurements from 2 to 300 K with dc field up to 70 kOe were performed using a Quantum Design SQUID VSM magnetometer on the grounded powders from the single crystals of the compounds. Alternative current (ac) magnetic susceptibility data were collected in a zero direct current (dc) field or 1 kOe dc field in the temperature range of 2-8 K, under an ac field of 2 Oe, oscillating at frequencies in the range of 1-1000 Hz. All magnetic data were corrected for the diamagnetism of the sample holder and of the diamagnetic contribution of the sample using Passcal's constants.

X-ray Crystallography. Single crystal X-ray crystallographic data were collected on a Bruker D8 Venture diffractometer with a CCD area detector (Mo-K α radiation, $\lambda = 0.71073 \text{ \AA}$) at 100 K. The unit cell parameters and data collection were determined by the APEXII program. Intensity data were corrected for Lorentz and polarization effects using SAINT^{S1}, scale variation for decay and absorption: a multi-scan absorption correction was applied with SADABS,^{S2} based on the intensities of symmetry-related reflections measured at different angular setting. The structures were solved by direct methods and refined by full-matrix least-squares method on F^2 using the SHELXTL^{S3} integrated in Olex 2.^{S4} Most hydrogen atoms were generated by geometrical considerations and constrained to idealized geometries and allowed to ride on their carrier atoms with an isotropic displacement parameter related to the equivalent displacement parameter of their carrier atoms. Hydrogen atoms of the organic ligands were refined as riding on the corresponding non-hydrogen atoms. Additional details of the data collections and structural refinement parameters are provided in Table 1. Selected bond lengths and angles of **1** and **2** are listed in Table S3 and S4. CCDC 2126529 and 2126530 is the supplementary crystallographic data for this paper. They can be obtained freely from the Cambridge Crystallographic Data Centre via www.ccdc.cam.ac.uk/data_request/cif.

Computation Methodology

CASSCF calculation

All calculations were carried out on the X-ray crystal structure using ORCA/4.2.1 code.^{S5,S6} The position of hydrogens were optimized using BP86 level of theory^{S7,S8} using def2-SVP^{S9} basis set for all atoms. For calculation of spin-Hamiltonian parameters (g, D and E) in complex **1** and **2**, here we have carried out complete active space self-consistent (CASSCF) method with an active space of CAS (7, 5) i.e., seven active electrons in the five active d-orbitals of Co(II) ion. All the SH parameters were computed at individual Co(II) centers and we have replaced other paramagnetic Co(II) ion by diamagnetic Zn(II) analogue. Using this active space, we have computed all 10 quartets and 40 doublet states in CI procedure. Here we have employed all electron DKH-def2-TZVPP^{S9} basis set for all the atoms. The scalar relativistic effects were accounted by Doughlas-Kroll-Hess (DKH) approximation as implemented in ORCA. To account the dynamic correlations, here we have performed N-electron valence second order perturbation theory (NEVPT2) on the top of the converged CASSCF wavefunction. Dispersion corrections have been taken care of by incorporating Grimme's atom-pairwise dispersion correction approach^{S11,S12} as implemented in ORCA. The spin-orbit coupling (SOC) effects were treated using Quasi-degenerate perturbation theory (QDPT) approach^{S13} where the spin-orbit mean field (SOMF) operator^{S14, S15} accounts for mixing of state with different multiplicities ($\Delta S = 0, \pm 1$) as implemented in the ORCA. Ab initio ligand field theory (AILFT) calculations were carried out along with CASSCF/NEVPT2 calculations to compute the one-electron ligand field energy (d-orbital splitting) and two electron integrals (Racah parameters).

CASSCF calculations were carried our alson in the MOLCAS code.^{S16} Here, we have employed the [ANO-RCC...5s4p2d1f] basis set for Co, the [ANO-RCC...4s3p] basis set for S, the [ANO-RCC...3s2p] basis set for N, O, and C atoms and the [ANO-RCC...2s] basis set for hydrogen. First, we carried out CASSCF calculations with an active space of seven electrons in five d-orbitals and calculated 10 quartet and 40 doublet spin-free states. In the next step, we mixed the 10 quartets and 40 doublets using the spin-orbit restricted active space spin interaction (SO-RASSI) to calculate the spin-orbit coupled states. The spin-orbit coupled states were then taken to the SINGLE_ANISO^{S17} program to calculate the SH parameters (D-tensor, g-tensor) and ab initio blockade barrier. Here we have turned on resolution of identity Cholesky decomposition (RICD) throughout the calculation to save the disk space.

POLY_ANISO Simulation

The exchange spectrum (dipolar and exchange contributions), along with the magnetic properties of the dinuclear compound, was simulated using POLY_ANISO^{S18} code based on obtained results from the ab initio calculations. The POLY_ANISO code has been successfully used to simulate the magnetic properties of highly anisotropic polynuclear complexes.^{S19-S24} Thus, we have computed the exchange coupling along with the SINGLE_ANISO values considering the lines (Heisenberg + Ising) model using the spin-Hamiltonian

$$\begin{aligned}\hat{H} = & D_{Co@1} \left[\hat{S}_z^2 - \frac{1}{3} S(S+1) \right] + E_{Co@1} [\hat{S}_x^2 - \hat{S}_y^2] + D_{Co@2} \left[\hat{S}_z^2 - \frac{1}{3} S(S+1) \right] \\ & + E_{Co@1} [\hat{S}_x^2 - \hat{S}_y^2] - J_{tot} \hat{S}_{Co@1} \hat{S}_{Co@2} + zJ'\end{aligned}$$

Where D, E, and J_{tot} represents the axial zero-field splitting, rhombic zero-field splitting and complete tensor of the exchange interaction between the two anisotropic Co(II) centers, respectively. The zJ' represents the intermolecular exchange term. The last term is used to obtain the reasonably good fit χT vs T at very low temperature.

Broken Symmetry DFT calculation

To compute the strength of the isotropic exchange coupling between the Co(II) centers in the complexes **1-2**, here we have carried out scalar relativistic DFT calculations. The scalar relativistic effects were accounted by Doughlas-Kroll-Hess (DKH) approximation as implemented in ORCA. Here, we have used DKH-def2-TZVP^{S9} basis set for all the atoms. All the broken-symmetry density functional theory (BS-DFT) calculations were carried out with B3LYP^{S10} functional and Grimme's D3BJ^{S11,S12} dispersion correction. The BS solutions were obtained by flipping the spin on one of the Co(II) centers of the dimer using "spinflip" approach as implemented in ORCA. The broken-symmetry solutions were verified by analyzing the nature of the spin density (spin-flip) on the individual paramagnetic centers. The exchange coupling was computed with the Yamaguchi formula^{S25,S26} by scaling the energy difference between the high-spin and broken-symmetry solutions according to their spin expectation values. To speed up the calculations, here we have used resolution-of-identity-chain-of-spheres RIJCOSX^{S27} as implemented in ORCA. A Tight convergence settings were used "tightscf" was used throughout the calculations for better numerical accuracy.

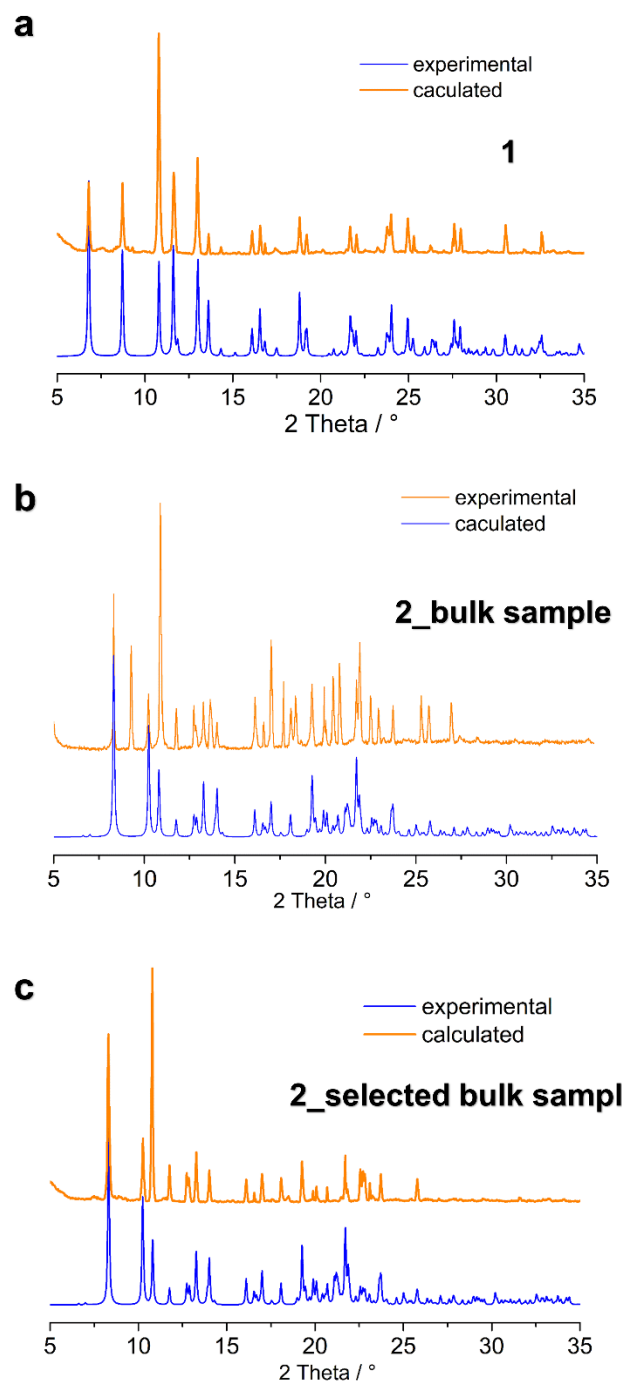


Figure S1. Comparison of the experimental PXRD patterns of **1** (a) and **2** (b) with the simulated patterns from their single crystal structures based on bulk sample. (c) Comparison of the experimental PXRD patterns of **2** with the simulated pattern based on the well-grounded hand-picked single crystals sample.

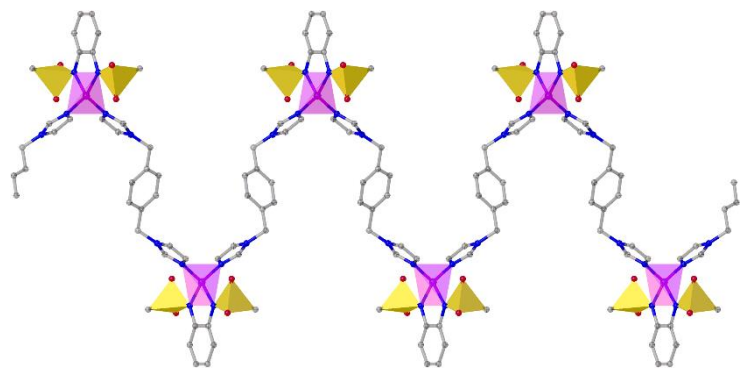


Figure S2. Crystal structure of the impurity in bulk sample of **2**.

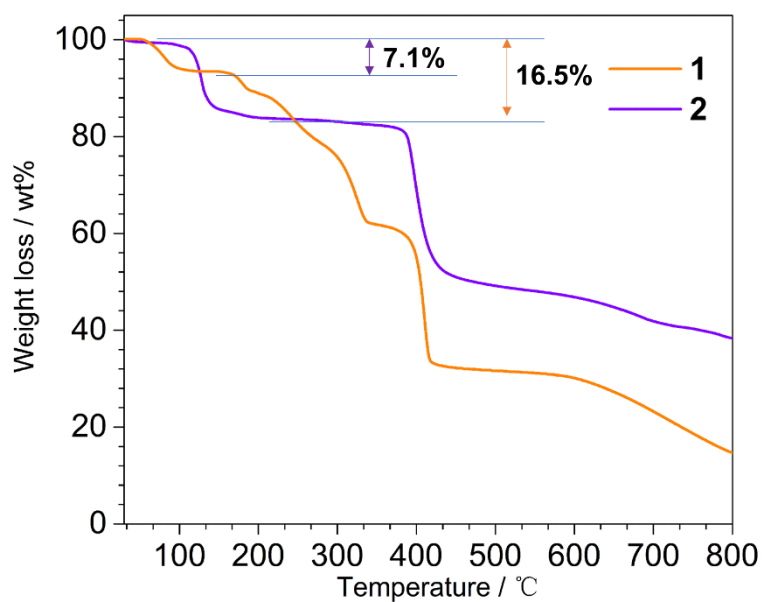


Figure S3. Thermogravimetric curves of **1** and **2** measured under the nitrogen atmosphere upon the continuous heating with the $10\text{ }^{\circ}\text{C}\cdot\text{min}^{-1}$ rate.

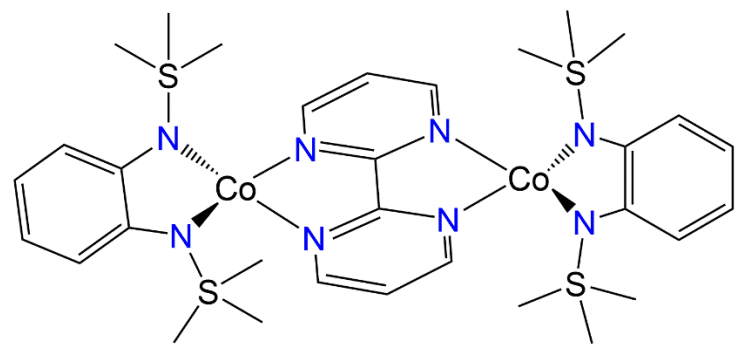


Figure S4. The designed cobalt dimer complex with tetrahedral Co^{2+} centers.

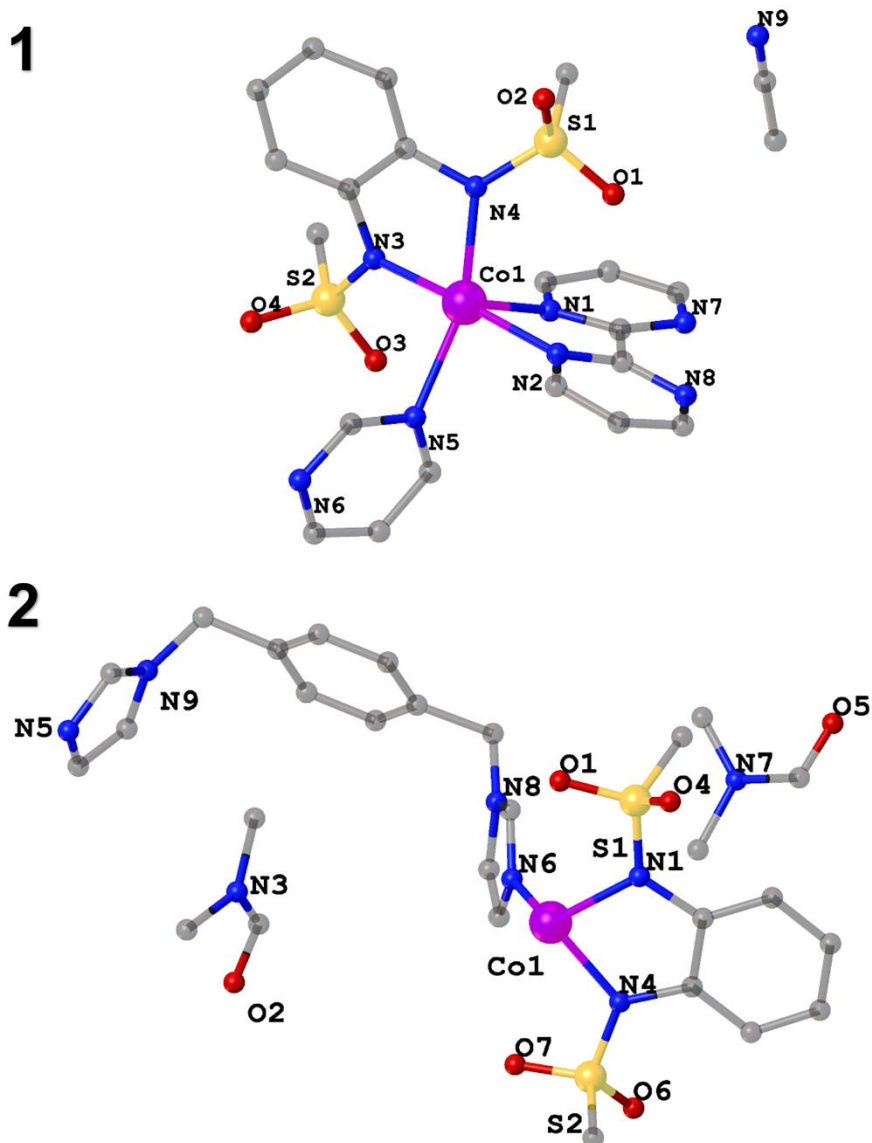


Figure S5. The asymmetric units of **1** and **2**.

Table S1. Selected bond lengths (\AA) and angles [$^\circ$] for **1**.

parameter	Value / \AA , $^\circ$
Co1-N1	2.116(3)
Co1-N2	2.141(3)
Co1-N3	2.093(3)
Co1-N4	2.069(3)
Co1-N5	2.202(3)
Co1-N6 ¹	2.206(3)
Co-N _{average}	2.138
N1-Co1-N2	76.51(13)
N1-Co1-N5	101.40(12)
N1-Co1-N6 ¹	171.73(13)
N2-Co1-N5	86.28(11)
N2-Co1-N6 ¹	95.70(12)
N3-Co1-N1	100.88(13)
N3-Co1-N2	175.82(12)
N4-Co1-N5	161.35(12)
Symmetry transformations used to generate equivalent atoms: ¹ 1-X,1-Y,1-Z	

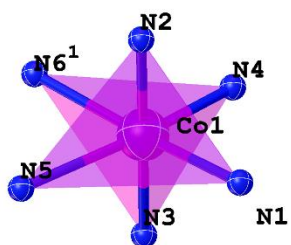


Table S2. Selected bond lengths (\AA) and angles [$^\circ$] for **2**.

parameter	Value / \AA , $^\circ$
Co1-N1	1.9840(14)
Co1-N4	1.9832(14)
Co1-N5 ¹	2.0145(15)
Co1-N6	2.0036(15)
Co1-N	1.996
N1-Co1-N5 ¹	114.30(6)
N1-Co1-N6	115.09(6)
N4-Co1-N1	81.04(6)
N4-Co1-N5 ¹	113.56(6)
N4-Co1-N6	112.62(6)
N6-Co1-N5 ¹	115.57(6)
Symmetry transformations used to generate equivalent atoms: ${}^1\bar{1}/2-X, 1/2-Y, 1-Z$	

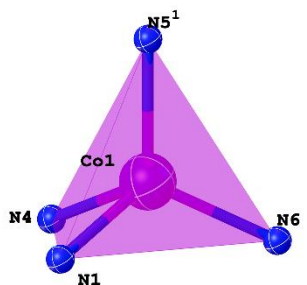


Table S3. Continuous Shape Measure (CSM) analysis for Co(II) ions in **1** and **2**.

Compound, Metal center	CSM parameters*					Determined coordination geometry	
	six-coordinated coordination sphere						
	HP-6	PPY-6	OC-6	TPR-6	JPPY-6		
1	29.044	23.706	6.505	15.856	25.394	OC-6	
four-coordinated coordination sphere							
2	SP-4	T-4	SS-4	vTBPY-4			
	29.314	2.235	9.410	3.081		T-4	

* CSM parameters for six-coordinated complexes: [S2](#)

HP-6 the parameter related to the hexagon (D_{6h})

PPY-6 the parameter related to the pentagonal pyramid (C_{5v})

OC-6 the parameter related to the octahedron (O_h)

TPR-6 the parameter related to the trigonal prism (D_{3h})

JPPY-6 the parameter related to the Johnson pentagonal pyramid (C_{5v})

SP-4 Square

T-4 Tetrahedron

SS-4 Seesaw or sawhorse‡ (cis-divacant octahedron)

vTBPY-4 Axially vacant trigonal bipyramide

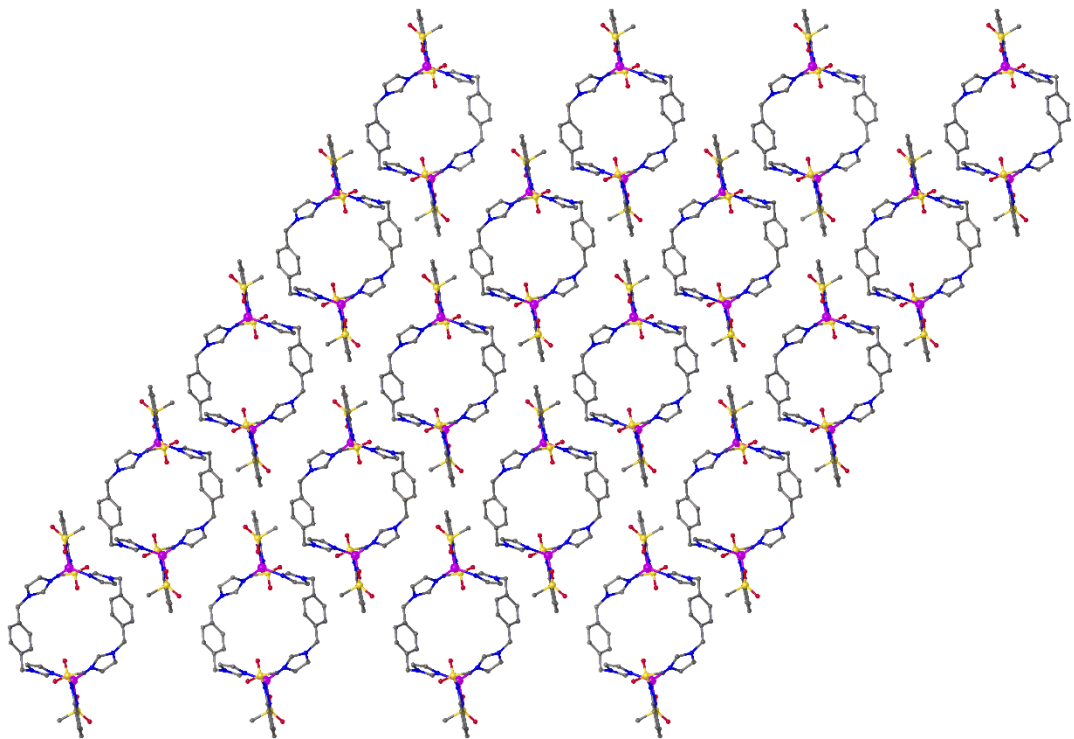


Figure S6. Packing diagram of the dicoordinate Co_2 metallocycle of **1** along crystallographic **b** axis.

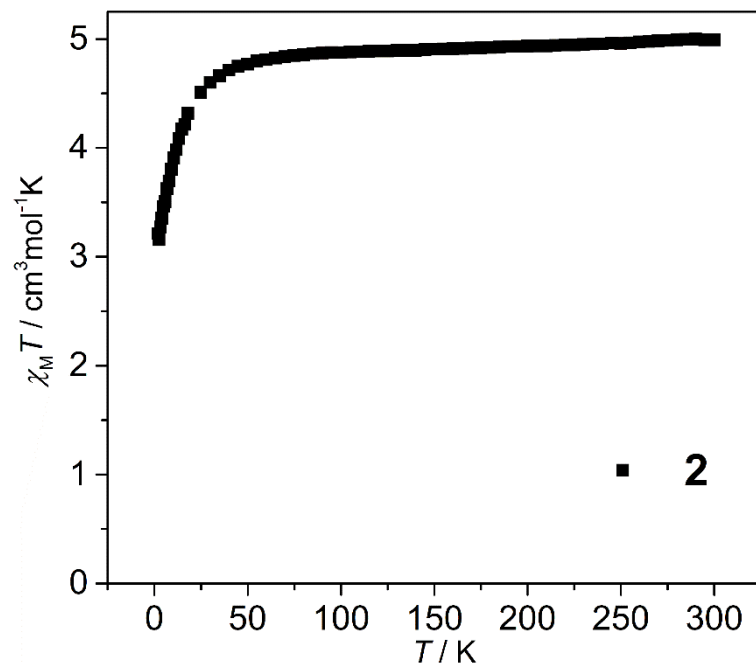


Figure S7. Variable-temperature magnetic susceptibility for **2** measured under applied dc field of 0.1 T.

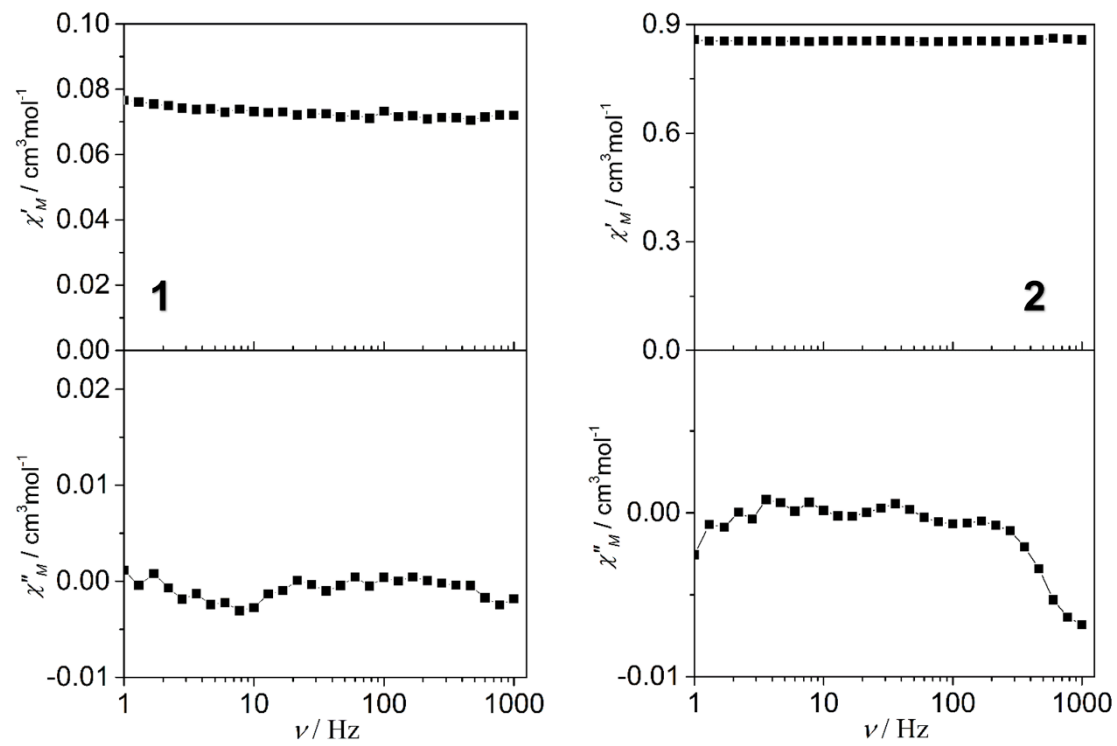


Figure S8. Frequency dependence of the in-phase (χ') and out-of-phase (χ'') ac susceptibilities measured under zero dc field at 2.0 K for **1** and **2**.

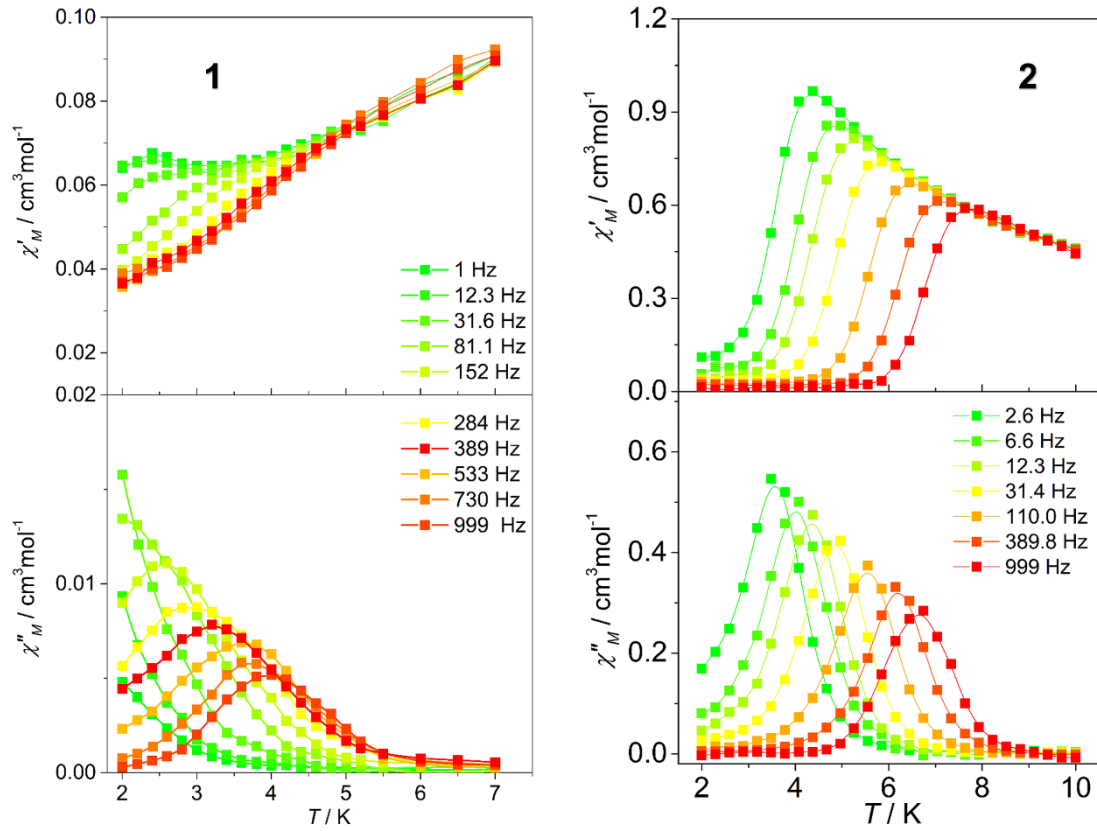


Figure S9. Temperature dependence of the in-phase (χ') and out-of-phase (χ'') part of the ac susceptibilities measured under 1 kOe dc field for **1** and **2**.

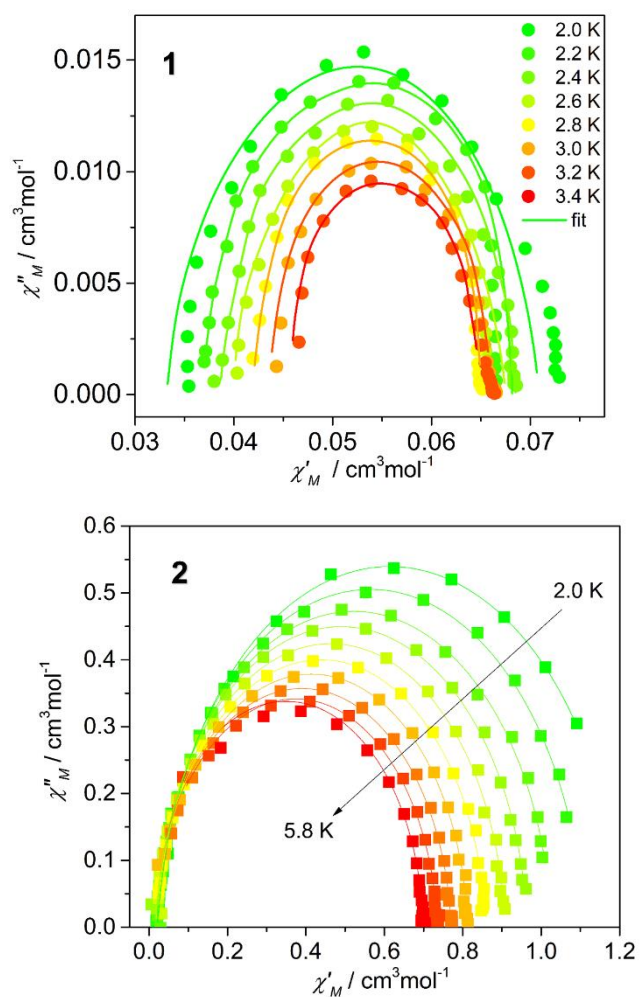


Figure S10. Cole-cole plot for **1** and **2** under 1000 Oe dc field. The solid lines are the best fits to the experiments with the generalized Debye model.

Table S4. Relaxation fitting parameters from the least-square fitting of the Cole-Cole plots of **1** according to the generalized Debye model.

T / K	τ / s	χ_s / cm ³ mol ⁻¹ K	χ_T / cm ³ mol ⁻¹ K	α
2.0	0.02593	0.88559	0.00402	0.1996
2.2	0.02069	0.84228	0.00339	0.20167
2.4	0.01473	0.7883	0.00264	0.17648
2.6	0.00944	0.73492	0.00196	0.18538
2.8	0.00556	0.69178	0.00157	0.16017
3.0	0.00306	0.64145	0.00121	0.12316
3.2	0.00155	0.61862	1E-3	0.1147
3.4	9.3E-4	0.57057	7.6E-4	0.00478

Table S5. Relaxation fitting parameters from the least-square fitting of the Cole-Cole plots of **2** according to the generalized Debye model.

T / K	τ / s	χ_s / cm ³ mol ⁻¹ K	χ_T / cm ³ mol ⁻¹ K	α
2.0	0.08285	0.01968	1.31523	0.08255
2.4	0.04469	0.02196	1.20739	0.05949
2.8	0.02459	0.02033	1.10862	0.04663
3.2	0.01392	0.01897	1.02591	0.04007
3.6	0.00815	0.01746	0.96335	0.03177
4.0	0.00483	0.02067	0.90638	0.02707
4.4	0.00283	0.01996	0.8571	0.02827
4.8	0.00162	0.01766	0.81173	0.02985
5.2	8.89907E-4	0.01021	0.76996	0.03886
5.6	4.92184E-4	0.01265	0.73448	0.03463

Table S6. CASSCF/NEVPT2 computed 10 spin-free quartets (red) and 40 spin-free doublets (blue) states along with the spin-orbit states for **1**. All the values are reported here in cm⁻¹.

Co@1							
SPIN-FREE STATES				SPIN-ORBIT STATES			
CASSCF		NEVPT2		CASSCF		NEVPT2	
0.0	49181.4	0.0	46350.8	0.00	36510.49	0.00	37125.95
700.4	49649.1	969.9	46433.0	138.23	37045.05	104.75	37969.88
1195.9	72012.1	1632.7	64714.0	818.62	37294.51	1048.64	38702.29
7281.6	72298.6	9528.6	65212.9	1087.23	37574.59	1264.94	38977.44
7684.6	73038.4	10132.7	65900.3	1483.28	37973.45	1841.54	39348.98
8352.8	74107.8	10955.5	67265.2	1609.31	47106.19	1962.48	42533.23
16002.4	74260.4	20554.6	67480.1	7528.14	47666.19	9244.24	43249.63
23543.5		22482.3		7568.25	48133.55	9711.65	43871.46
24491.6		23560.8		7933.79	48570.39	9742.74	45321.70
25526.2		24870.3		7990.48	49229.38	10306.25	46322.89
13530.2		9021.9		8599.18	49565.76	10364.93	46645.17
14743.7		10675.6		8686.53	49963.72	10911.86	46710.61
19600.3		17832.5		13790.76	72286.31	11131.75	64950.18
19944.9		18405.6		15001.51	72625.90	11215.22	65472.96
20251.7		18843.8		16301.15	73360.97	17998.99	66176.30
20425.2		19125.0		16305.42	74322.56	18566.40	67439.22
20731.2		19444.5		19783.76	74705.90	18989.34	67853.77
21032.7		19976.8		20137.88		19414.97	
25618.7		22721.4		20465.55		19744.90	
25757.2		22800.7		20812.69		20239.09	
26005.5		23162.3		21119.69		20809.88	
26179.5		26561.7		21433.24		20853.68	
28945.7		28532.2		23635.32		22123.88	
29184.5		28621.2		23718.33		22406.49	
29931.9		30103.3		24519.44		22809.61	
30093.4		30166.5		24678.69		23181.53	
30388.8		30455.6		25342.90		23309.60	
30747.1		31058.1		25637.86		23919.86	
32513.5		32685.7		25792.13		24172.20	
32591.2		32846.7		26393.95		25189.76	
35179.8		35106.7		26595.87		25275.69	
35717.4		35867.7		26999.98		26838.91	
35861.9		35905.2		29230.28		28720.90	
36077.5		36767.5		29576.61		28991.04	
36556.0		37614.6		30238.13		30321.77	
36902.7		38455.8		30388.35		30418.19	
37240.7		38769.6		30692.84		30698.97	
37367.2		38839.0		31033.29		31280.75	
46913.3		42361.2		32794.52		32920.59	
47359.9		43006.3		32947.96		33126.78	
47782.3		43583.4		35365.19		35271.15	
48286.4		45093.6		35880.21		35986.87	
49005.4		46154.4		36012.88		36169.93	

Co@2							
SPIN-FREE STATES				SPIN-ORBIT STATES			
CASSCF		NEVPT2		CASSCF		NEVPT2	
0.0	72298.6	0.0	65213.0	0.00	37574.60	0.0	38977.4
700.4	73038.4	969.8	65900.3	138.23	37973.46	104.8	39349.0
1195.9	74107.8	1632.7	67265.2	818.61	47106.19	1048.6	42533.2
7281.6	74260.4	9528.7	67480.1	1087.23	47666.19	1264.9	43249.6
7684.6		10132.7		1483.27	48133.55	1841.5	43871.5
8352.8		10955.5		1609.31	48570.39	1962.5	45321.7
16002.4		20554.6		7528.14	49229.38	9244.2	46322.9
23543.5		22482.3		7568.26	49565.76	9711.7	46645.2
24491.6		23560.8		7933.80	49963.73	9742.8	46710.6
25526.2		24870.3		7990.48	72286.31	10306.3	64950.2
13530.2		9021.9		8599.18	72625.91	10364.9	65473.0
14743.7		10675.6		8686.53	73360.97	10911.9	66176.3
19600.3		17832.5		13790.76	74322.56	11131.8	67439.2
19944.9		18405.6		15001.50	74705.90	11215.2	67853.8
20251.7		18843.8		16301.16		17999.0	
20425.2		19124.9		16305.43		18566.4	
20731.2		19444.5		19783.76		18989.3	
21032.6		19976.8		20137.88		19415.0	
25618.7		22721.4		20465.55		19744.9	
25757.2		22800.7		20812.69		20239.1	
26005.5		23162.3		21119.69		20809.9	
26179.5		26561.7		21433.24		20853.7	
28945.7		28532.2		23635.32		22123.9	
29184.5		28621.2		23718.33		22406.5	
29931.9		30103.3		24519.44		22809.6	
30093.4		30166.5		24678.69		23181.5	
30388.8		30455.6		25342.90		23309.6	
30747.1		31058.1		25637.86		23919.9	
32513.5		32685.7		25792.14		24172.2	
32591.2		32846.7		26393.95		25189.8	
35179.8		35106.7		26595.87		25275.7	
35717.4		35867.7		26999.98		26838.9	
35861.9		35905.2		29230.28		28720.9	
36077.5		36767.5		29576.62		28991.0	
36556.0		37614.6		30238.13		30321.8	
36902.7		38455.8		30388.35		30418.2	
37240.7		38769.6		30692.85		30699.0	
37367.2		38839.0		31033.29		31280.8	
46913.3		42361.2		32794.52		32920.6	
47359.9		43006.3		32947.96		33126.8	
47782.3		43583.4		35365.20		35271.2	
48286.4		45093.6		35880.21		35986.9	
49005.5		46154.4		36012.88		36169.9	
49181.4		46350.8		36510.49		37126.0	

49649.1		46433.0		37045.05		37969.9	
72012.1		64714.0		37294.52		38702.3	

Table S7. CASSCF/NEVPT2 computed 10 spin-free quartets (red) and 40 spin-free doublet (blue) states along with the spin-orbit states for complex **2**. All the values are reported here in cm⁻¹.

Co@1							
SPIN-FREE STATES				SPIN-ORBIT STATES			
CASSCF	NEVPT2	CASSCF	NEVPT2	CASSCF	NEVPT2	CASSCF	NEVPT2
0.0	47874.0	0.0	44077.2	0.00	33027.20	0.00	32636.13
3126.9	48019.8	3766.7	44619.9	29.93	33443.91	28.11	33876.65
5200.7	68541.2	6946.5	59866.4	3138.88	34074.05	3783.01	34229.79
5288.2	69430.0	7052.6	61431.9	3267.75	35634.57	3886.28	36069.58
6678.3	71649.6	8656.7	63964.5	5077.78	35890.79	6826.15	36640.39
8509.5	71884.3	10641.6	64222.0	5294.76	45496.64	7012.74	41051.50
8701.5	73043.2	11140.3	65749.6	5354.67	46050.55	7080.46	41463.03
22459.1		21184.7		5396.04	46378.79	7123.96	42151.76
22763.4		21299.9		6806.75	47274.60	8753.88	43277.61
24959.6		23819.8		6933.48	47617.45	8871.19	43687.68
19829.9		17787.4		8305.70	48037.50	10495.10	44225.60
19894.2		18197.2		8631.11	48205.73	10761.02	44761.16
20040.8		18252.7		9001.31	68688.75	11354.74	60008.18
20106.9		18557.0		9257.12	69600.47	11554.78	61583.08
20589.6		19163.5		19548.10	71801.20	17650.01	64102.23
21477.7		20945.6		19961.41	72020.45	18248.94	64348.02
22650.9		21946.3		20130.64	73245.10	18415.35	65925.50
23191.3		22711.3		20401.06		18713.23	
23998.5		23970.1		20757.34		19300.34	
25812.8		24355.2		21786.22		21077.60	
26572.5		24966.3		22421.56		21156.04	
26676.3		25570.9		22485.81		21179.38	
26795.8		25871.9		22680.20		21336.90	
27500.8		25916.7		22822.69		21509.44	
28228.9		26641.5		22936.74		21982.64	
28847.9		27791.2		23279.03		22789.12	
29740.3		28025.5		24166.07		23622.03	
30048.9		29512.8		24903.26		23898.92	
30274.0		29812.3		25068.36		24245.68	
30438.5		30417.9		25937.27		24464.25	
31294.7		30679.3		26589.49		25094.07	
31891.9		31247.5		26830.49		25606.40	
32413.9		31713.1		27235.51		26146.52	
32817.7		32430.6		27764.56		26257.30	
33242.2		33734.2		28306.34		26755.23	
33866.0		34024.7		29069.14		27908.80	
35393.2		35872.1		29792.79		28219.33	
35559.7		36399.4		30074.82		29565.16	

45375.5		40947.7		30492.52		30041.97	
45940.4		41361.9		30856.24		30635.42	
46249.6		42041.9		31429.65		30803.31	
47156.6		43173.0		31949.14		31281.84	
47493.7		43582.6		32660.93		31971.25	

Co@2							
SPIN-FREE STATES				SPIN-ORBIT STATES			
CASSCF		NEVPT2		CASSCF		NEVPT2	
0.0	48019.8	0.0	44619.9	0.00	33443.90	0.00	33876.65
3126.9	68541.2	3766.7	59866.4	29.93	34074.05	28.11	34229.79
5200.7	69430.0	6946.5	61431.9	3138.86	35634.56	3783.00	36069.58
5288.2	71649.6	7052.6	63964.4	3267.74	35890.79	3886.27	36640.38
6678.3	71884.3	8656.7	64222.0	5077.78	45496.64	6826.15	41051.50
8509.5	73043.2	10641.6	65749.5	5294.76	46050.54	7012.74	41463.02
8701.5		11140.3		5354.67	46378.80	7080.46	42151.76
22459.1		21184.7		5396.03	47274.60	7123.96	43277.60
22763.4		21299.9		6806.74	47617.45	8753.88	43687.67
24959.6		23819.8		6933.48	48037.49	8871.19	44225.60
19829.9		17787.4		8305.69	48205.73	10495.10	44761.16
19894.2		18197.2		8631.10	68688.75	10761.02	60008.17
20040.8		18252.7		9001.31	69600.47	11354.74	61583.09
20106.9		18557.0		9257.12	71801.19	11554.77	64102.23
20589.6		19163.5		19548.09	72020.45	17650.00	64348.01
21477.7		20945.6		19961.41	73245.09	18248.93	65925.50
22650.9		21946.3		20130.64		18415.34	
23191.3		22711.3		20401.06		18713.24	
23998.5		23970.1		20757.33		19300.33	
25812.8		24355.2		21786.21		21077.61	
26572.5		24966.3		22421.56		21156.03	
26676.3		25570.9		22485.80		21179.38	
26795.8		25871.9		22680.19		21336.90	
27500.8		25916.7		22822.69		21509.45	
28228.9		26641.5		22936.75		21982.63	
28847.9		27791.2		23279.03		22789.13	
29740.3		28025.5		24166.07		23622.02	
30048.8		29512.8		24903.24		23898.91	
30274.0		29812.4		25068.35		24245.67	
30438.5		30417.9		25937.26		24464.24	
31294.7		30679.3		26589.49		25094.08	
31891.9		31247.5		26830.49		25606.40	
32413.9		31713.1		27235.51		26146.51	
32817.7		32430.6		27764.55		26257.29	
33242.2		33734.2		28306.35		26755.24	
33866.0		34024.7		29069.15		27908.80	
35393.2		35872.1		29792.79		28219.33	
35559.7		36399.4		30074.81		29565.15	
45375.5		40947.7		30492.52		30041.98	
45940.4		41361.9		30856.25		30635.42	

Supporting Information

46249.6		42041.9		31429.65		30803.31	
47156.6		43173.0		31949.14		31281.83	
47493.7		43582.6		32660.93		31971.24	
47874.0		44077.2		33027.20		32636.12	

Table S8. CASSCF (7,5)+NEVPT2 computed Spin-Hamiltonian parameter (g , D , $|E/D|$) along with wave function decomposition analysis for complexes **1** and **2**. All these data obtained from ORCA code.

Parameters		1		2	
		CASSCF	NEVPT2	CASSCF	NEVPT2
		Contribution to D (cm^{-1})			
$^4\text{T}_{1g}$	0.0	0.0	0.0	0.0	0.0
	38.9	31.1	17.5	14.6	
	23.0	17.5	12.0	-18.4	
D	EHA	65.69	49.43	13.12	-12.36
	2PT	67.38	48.00	15.27	13.37
$ E/D $	EHA	0.18	0.20	0.31	0.31
	2PT	0.30	0.29	0.28	0.32
g_{\min}		2.0188	2.0317	2.1854	2.1420
g_{mid}		2.4532	2.3857	2.2776	2.2125
g_{\max}		2.7673	2.6544	2.3797	2.3221
		KD1: 49% $ 3/2; \pm 1/2\rangle$ + 45% $ 3/2; \pm 3/2\rangle$		KD1: 92% $ 3/2; \pm 3/2\rangle$ + 6% $ 3/2; \pm 1/2\rangle$	
g_{\min}		2.0443	1.9075	1.6453	1.5056
g_{mid}		3.4628	3.2719	2.3824	2.0912
g_{\max}		6.7450	6.6015	6.4382	6.4021
		KD1: 50% $ 3/2; \pm 3/2\rangle$ + 47% $ 3/2; \pm 1/2\rangle$		KD1: 91% $ 3/2; \pm 1/2\rangle$ + 5% $ 3/2; \pm 3/2\rangle$	
g_{\min}		1.4022	1.4517	1.7018	1.7721
g_{mid}		1.5079	1.4901	2.1716	2.3334

Supporting Information

g_{\max}	5.7410	5.8159	6.0162	5.7897
<i>EHA : Effective Hamiltonian approach ; 2PT : Second order perturbation Theory</i>				

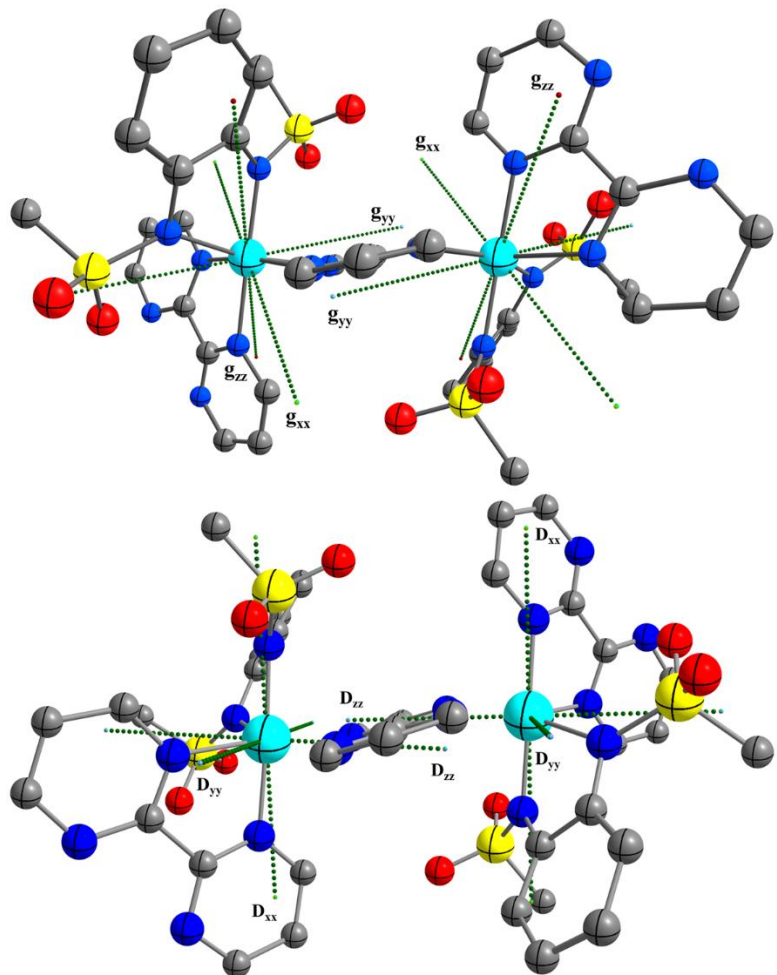


Figure S11. NEVPT2 computed orientation of computed effective g-tensor and D-tensor for complex **1**. Color code: Co(cyan), N (blue), S(yellow), C (grey), O(red). The hydrogens are omitted for clarity.

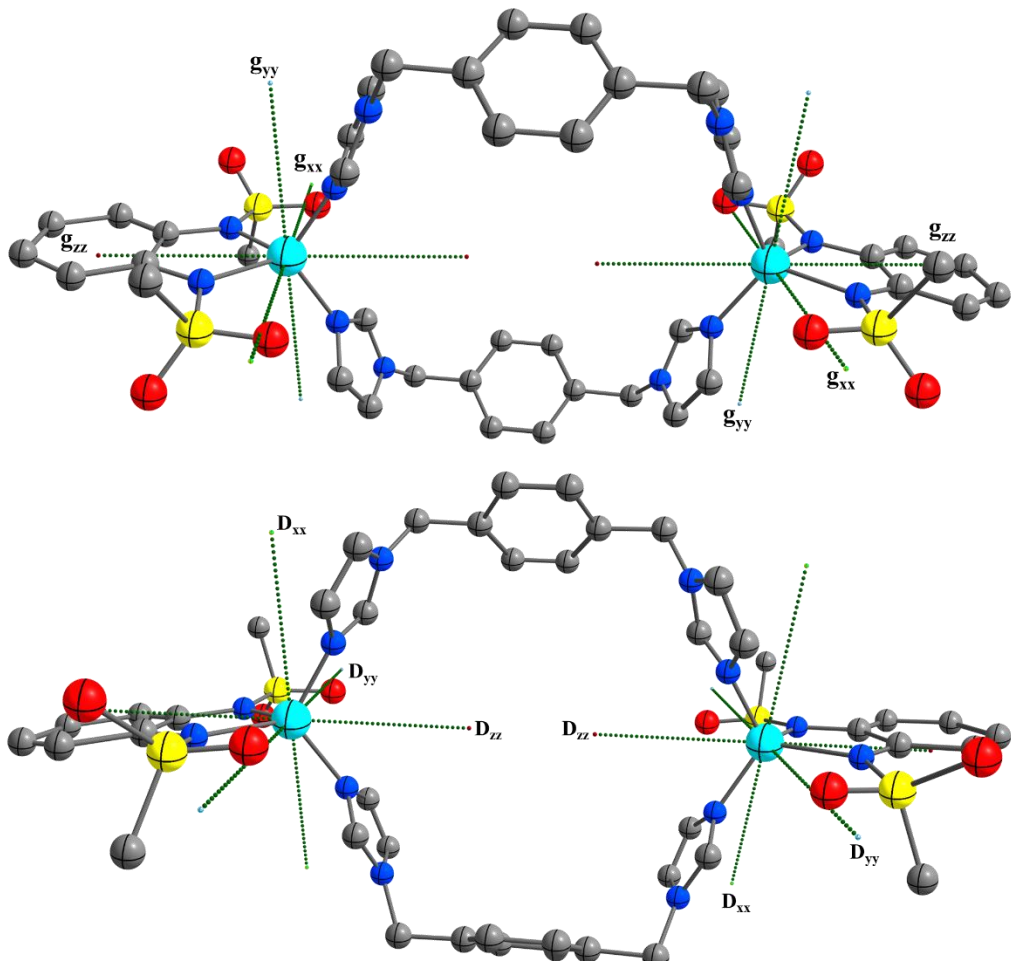


Figure S12. NEVPT2 computed orientation of computed effective g-tensor and D-tensor for complex **2**. Color code: Co(cyan), N (blue), S(yellow), C (grey), O(red). The hydrogens are omitted for clarity.

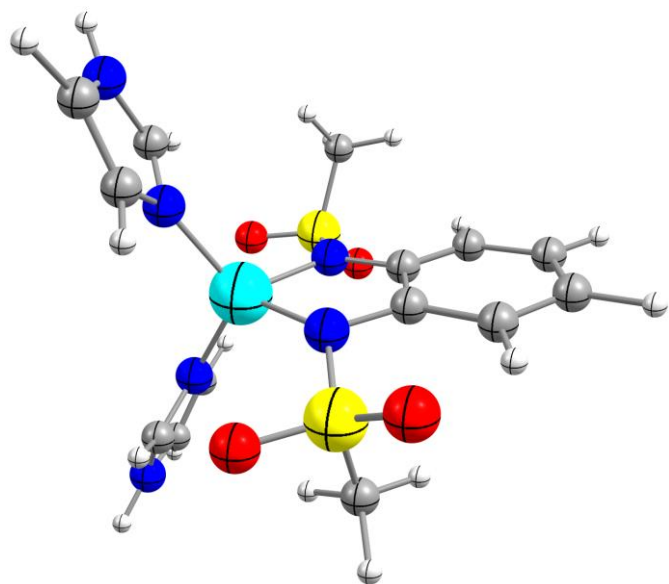


Figure S13. Model complex prepared to study the variation in spin-Hamiltonian parameters with change in $\angle\text{N-Co-N}$. Color code: Co (cyan); N (blue), O (red), S (yellow), C (grey).

Table S9. NEVPT2 computed variation of the spin-Hamiltonian parameters (D and |E/D|) with change in \angle N-Co-N for model complex **2**.

\angle N-Co-N (°)	D (cm ⁻¹)	E/D
80	-59.6	0.01
85	-48.9	0.02
90	-40.1	0.03
95	-32.7	0.05
100	-26.4	0.08
105	-21.2	0.12
110	-16.7	0.19
115	-12.4	0.30

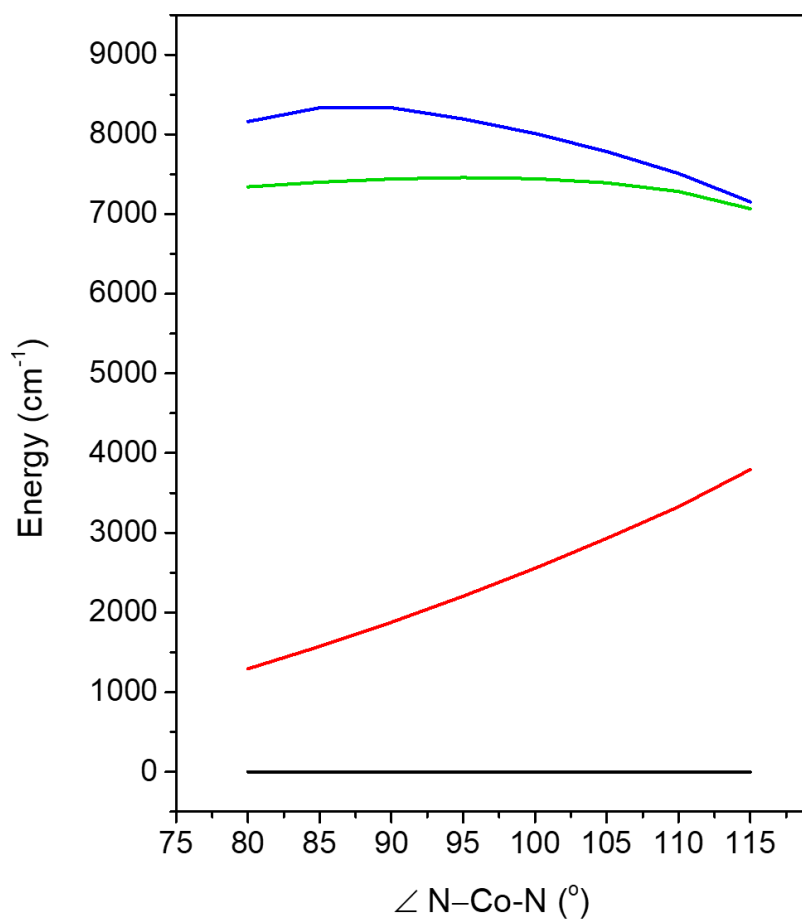


Figure S14. NEVPT2 computed variation of energy of the first three excited states (in cm^{-1}) with change in the $\angle \text{N-Co-N}$ ($^{\circ}$) for model complex **2** (black line: ground state; red, green, blue: first, second and third excited states respectively)

Table S10. Energies (in cm^{-1}) of spin-free ground and first excited state of the $S = 3/2$ states spanned by the d^7 configuration in **1** and **2**, and the constituting electronic configurations.

Complex		Energy (cm^{-1})	Electronic configuration
1	${}^4\text{T}_{1g}$	0.0	0.39 $(d_{xy})^2(d_{yz})^1(d_{z^2})^2(d_{xz})^1(d_{x^2-y^2})^1 +$ 0.26 $(d_{xy})^1(d_{yz})^1(d_{z^2})^2(d_{xz})^1(d_{x^2-y^2})^2$
		969.9	0.50 $(d_{xy})^2(d_{yz})^1(d_{z^2})^2(d_{xz})^1(d_{x^2-y^2})^1 +$ 0.17 $(d_{xy})^1(d_{yz})^1(d_{z^2})^2(d_{xz})^1(d_{x^2-y^2})^2$
		1632.7	0.36 $(d_{xy})^2(d_{yz})^1(d_{z^2})^1(d_{xz})^2(d_{x^2-y^2})^1 +$ 0.27 $(d_{xy})^1(d_{yz})^1(d_{z^2})^1(d_{xz})^2(d_{x^2-y^2})^2$
2	${}^4\text{T}_{1g}$	0.0	0.86 $(d_{xy})^2(d_{yz})^1(d_{z^2})^2(d_{xz})^1(d_{x^2-y^2})^1 +$ 0.07 $(d_{xy})^1(d_{yz})^1(d_{z^2})^2(d_{xz})^1(d_{x^2-y^2})^2$
		3766.7	0.88 $(d_{xy})^1(d_{yz})^1(d_{z^2})^2(d_{xz})^1(d_{x^2-y^2})^2 +$ 0.07 $(d_{xy})^2(d_{yz})^1(d_{z^2})^2(d_{xz})^1(d_{x^2-y^2})^1$
		6946.5	0.49 $(d_{xy})^2(d_{yz})^2(d_{z^2})^1(d_{xz})^1(d_{x^2-y^2})^1 +$ 0.30 $(d_{xy})^1(d_{yz})^2(d_{z^2})^1(d_{xz})^1(d_{x^2-y^2})^2$

Table S11. Energies (in cm⁻¹) of spin-free of the ground and the first excited states of the $S = 3/2$ states spanned by the d⁷ configuration in magneto-structural correlation developed for complex **2**, and the constituting electronic configurations.

$\angle \text{N-Co-N}(\circ)$	Energy (cm ⁻¹)		Electronic configuration
80	⁴ A ₂	0.0	0.82 (d_{xy}) ² (d_{yz}) ¹ (d_{z^2}) ² (d_{xz}) ¹ ($d_{x^2-y^2}$) ¹ + 0.16 (d_{xy}) ¹ (d_{yz}) ¹ (d_{z^2}) ² (d_{xz}) ¹ ($d_{x^2-y^2}$) ²
		1294.4 (⁴ A ₁)	0.82 (d_{xy}) ¹ (d_{yz}) ¹ (d_{z^2}) ² (d_{xz}) ¹ ($d_{x^2-y^2}$) ² + 0.16 (d_{xy}) ² (d_{yz}) ¹ (d_{z^2}) ² (d_{xz}) ¹ ($d_{x^2-y^2}$) ¹
	⁴ T ₂	7343 (⁴ B ₁)	0.63 (d_{xy}) ² (d_{yz}) ² (d_{z^2}) ¹ (d_{xz}) ¹ ($d_{x^2-y^2}$) ¹ + 0.16 (d_{xy}) ¹ (d_{yz}) ² (d_{z^2}) ¹ (d_{xz}) ¹ ($d_{x^2-y^2}$) ²
		8161.9 (⁴ B ₂)	0.54 (d_{xy}) ¹ (d_{yz}) ² (d_{z^2}) ¹ (d_{xz}) ¹ ($d_{x^2-y^2}$) ² + 0.17 (d_{xy}) ² (d_{yz}) ² (d_{z^2}) ¹ (d_{xz}) ¹ ($d_{x^2-y^2}$) ¹
	85	⁴ A ₂	0.82 (d_{xy}) ² (d_{yz}) ¹ (d_{z^2}) ² (d_{xz}) ¹ ($d_{x^2-y^2}$) ¹ + 0.17 (d_{xy}) ¹ (d_{yz}) ¹ (d_{z^2}) ² (d_{xz}) ¹ ($d_{x^2-y^2}$) ²
		1574.7 (⁴ A ₁)	0.82 (d_{xy}) ¹ (d_{yz}) ¹ (d_{z^2}) ² (d_{xz}) ¹ ($d_{x^2-y^2}$) ² + 0.17 (d_{xy}) ² (d_{yz}) ¹ (d_{z^2}) ² (d_{xz}) ¹ ($d_{x^2-y^2}$) ¹
		⁴ T ₂	0.63 (d_{xy}) ² (d_{yz}) ² (d_{z^2}) ¹ (d_{xz}) ¹ ($d_{x^2-y^2}$) ¹ + 0.16 (d_{xy}) ¹ (d_{yz}) ² (d_{z^2}) ¹ (d_{xz}) ¹ ($d_{x^2-y^2}$) ²
		8334.6 (⁴ B ₂)	0.53 (d_{xy}) ² (d_{yz}) ¹ (d_{z^2}) ¹ (d_{xz}) ² ($d_{x^2-y^2}$) ¹ + 0.19 (d_{xy}) ¹ (d_{yz}) ¹ (d_{z^2}) ¹ (d_{xz}) ² ($d_{x^2-y^2}$) ²

90	⁴ A ₂	0.0	$0.82 (d_{xy})^2(d_{yz})^1(d_{z^2})^2(d_{xz})^1(d_{x^2-y^2})^1 +$ $0.17 (d_{xy})^1(d_{yz})^1(d_{z^2})^2(d_{xz})^1(d_{x^2-y^2})^2$
	⁴ T ₂	1878 (⁴ A ₁)	$0.81 (d_{xy})^1(d_{yz})^1(d_{z^2})^2(d_{xz})^1(d_{x^2-y^2})^2 +$ $0.17 (d_{xy})^2(d_{yz})^1(d_{z^2})^2(d_{xz})^1(d_{x^2-y^2})^2$
		7441.3 (⁴ B ₁)	$0.63 (d_{xy})^2(d_{yz})^2(d_{z^2})^1(d_{xz})^1(d_{x^2-y^2})^1 +$ $0.16 (d_{xy})^1(d_{yz})^2(d_{z^2})^1(d_{xz})^1(d_{x^2-y^2})^2$
		8335.5 (⁴ B ₂)	$0.58 (d_{xy})^2(d_{yz})^1(d_{z^2})^1(d_{xz})^2(d_{x^2-y^2})^1 +$ $0.16 (d_{xy})^1(d_{yz})^1(d_{z^2})^1(d_{xz})^2(d_{x^2-y^2})^2$
95	⁴ A ₂	0.0	$0.81 (d_{xy})^2(d_{yz})^1(d_{z^2})^2(d_{xz})^1(d_{x^2-y^2})^1 +$ $0.17 (d_{xy})^1(d_{yz})^1(d_{z^2})^2(d_{xz})^1(d_{x^2-y^2})^2$
	⁴ T ₂	2204.6 (⁴ A ₁)	$0.81 (d_{xy})^1(d_{yz})^1(d_{z^2})^2(d_{xz})^1(d_{x^2-y^2})^2 +$ $0.17 (d_{xy})^2(d_{yz})^1(d_{z^2})^2(d_{xz})^1(d_{x^2-y^2})^1$
		7458.5 (⁴ B ₁)	$0.63 (d_{xy})^2(d_{yz})^2(d_{z^2})^1(d_{xz})^1(d_{x^2-y^2})^1 +$ $0.15 (d_{xy})^1(d_{yz})^2(d_{z^2})^1(d_{xz})^1(d_{x^2-y^2})^2$
		8194.4 (⁴ B ₂)	$0.58 (d_{xy})^2(d_{yz})^1(d_{z^2})^1(d_{xz})^2(d_{x^2-y^2})^1 +$ $0.16 (d_{xy})^1(d_{yz})^1(d_{z^2})^1(d_{xz})^2(d_{x^2-y^2})^2$
100	⁴ A ₂	0.0	$0.81 (d_{xy})^2(d_{yz})^1(d_{z^2})^2(d_{xz})^1(d_{x^2-y^2})^1 +$ $0.18 (d_{xy})^1(d_{yz})^1(d_{z^2})^2(d_{xz})^1(d_{x^2-y^2})^2$
	⁴ T ₂	2555.4 (⁴ A ₁)	$0.81 (d_{xy})^2(d_{yz})^2(d_{z^2})^1(d_{xz})^1(d_{x^2-y^2})^1 +$ $0.18 (d_{xy})^1(d_{yz})^2(d_{z^2})^1(d_{xz})^1(d_{x^2-y^2})^2$

		7446 (${}^4\text{B}_1$)	$0.62(d_{xy})^2(d_{yz})^2(d_{z^2})^1(d_{xz})^1(d_{x^2-y^2})^1 +$ $0.17(d_{xy})^1(d_{yz})^1(d_{z^2})^2(d_{xz})^2(d_{x^2-y^2})^1$
		8012.8 (${}^4\text{B}_2$)	$0.58(d_{xy})^2(d_{yz})^1(d_{z^2})^1(d_{xz})^2(d_{x^2-y^2})^1 +$ $0.16(d_{xy})^1(d_{yz})^1(d_{z^2})^1(d_{xz})^2(d_{x^2-y^2})^2$
105	${}^4\text{A}_2$	0.0	$0.80(d_{xy})^2(d_{yz})^1(d_{z^2})^2(d_{xz})^1(d_{x^2-y^2})^1 +$ $0.18(d_{xy})^1(d_{yz})^1(d_{z^2})^2(d_{xz})^1(d_{x^2-y^2})^2$
		2930.1 (${}^4\text{A}_1$)	$0.80(d_{xy})^1(d_{yz})^1(d_{z^2})^2(d_{xz})^1(d_{x^2-y^2})^2 +$ $0.18(d_{xy})^2(d_{yz})^1(d_{z^2})^2(d_{xz})^1(d_{x^2-y^2})^1$
		7393.4 (${}^4\text{B}_1$)	$0.60(d_{xy})^2(d_{yz})^2(d_{z^2})^1(d_{xz})^1(d_{x^2-y^2})^1 +$ $0.20(d_{xy})^1(d_{yz})^1(d_{z^2})^2(d_{xz})^2(d_{x^2-y^2})^1$
	${}^4\text{T}_2$	7785.4 (${}^4\text{B}_2$)	$0.58(d_{xy})^2(d_{yz})^1(d_{z^2})^1(d_{xz})^2(d_{x^2-y^2})^1 +$ $0.16(d_{xy})^1(d_{yz})^1(d_{z^2})^1(d_{xz})^2(d_{x^2-y^2})^2$
		0.0	$0.80(d_{xy})^2(d_{yz})^1(d_{z^2})^2(d_{xz})^1(d_{x^2-y^2})^1 +$ $0.18(d_{xy})^1(d_{yz})^1(d_{z^2})^2(d_{xz})^1(d_{x^2-y^2})^2$
		3328.1 (${}^4\text{A}_1$)	$0.80(d_{xy})^1(d_{yz})^1(d_{z^2})^2(d_{xz})^1(d_{x^2-y^2})^2 +$ $0.18(d_{xy})^2(d_{yz})^1(d_{z^2})^2(d_{xz})^1(d_{x^2-y^2})^2$
110	${}^4\text{T}_2$	7284.9 (${}^4\text{B}_1$)	$0.56(d_{xy})^2(d_{yz})^2(d_{z^2})^1(d_{xz})^1(d_{x^2-y^2})^1 +$ $0.25(d_{xy})^1(d_{yz})^1(d_{z^2})^2(d_{xz})^2(d_{x^2-y^2})^1$
		7511.5 (${}^4\text{B}_2$)	$0.58(d_{xy})^2(d_{yz})^1(d_{z^2})^1(d_{xz})^2(d_{x^2-y^2})^1 +$ $0.17(d_{xy})^1(d_{yz})^1(d_{z^2})^1(d_{xz})^2(d_{x^2-y^2})^2$

115	⁴ A ₂	0.0	$0.79 \ (d_{xy})^2(d_{yz})^1(d_{z^2})^2(d_{xz})^1(d_{x^2-y^2})^1 +$ $0.18 \ (d_{xy})^1(d_{yz})^1(d_{z^2})^2(d_{xz})^1(d_{x^2-y^2})^2$
		3793.9 (⁴ A ₁)	$0.80 \ (d_{xy})^1(d_{yz})^2(d_{z^2})^1(d_{xz})^1(d_{x^2-y^2})^2 +$ $0.19 \ (d_{xy})^2(d_{yz})^1(d_{z^2})^2(d_{xz})^1(d_{x^2-y^2})^1$
	⁴ T ₂	7067.9 (⁴ B ₁)	$0.51 \ (d_{xy})^2(d_{yz})^2(d_{z^2})^1(d_{xz})^1(d_{x^2-y^2})^1 +$ $0.30 \ (d_{xy})^1(d_{yz})^1(d_{z^2})^2(d_{xz})^2(d_{x^2-y^2})^1$
		7154.8 (⁴ B ₂)	$0.58 \ (d_{xy})^2(d_{yz})^1(d_{z^2})^1(d_{xz})^2(d_{x^2-y^2})^1 +$ $0.18 \ (d_{xy})^1(d_{yz})^1(d_{z^2})^1(d_{xz})^2(d_{x^2-y^2})^2$

Table S12. AILFT computed d-orbital ordering in the magneto-structural correlation developed for complex **2**.

$\angle\text{N-Co-N}$	80	85	90	95	100	105	110	115
d_{yz}	0.0	0.0	0.0	0.0	0.0	0.0	0.0	0.0
d_{xz}	1116.5	926.3	760.1	617.5	432.4	278.9	128.2	32.1
d_{xy}	1175.2	1446.2	1758.5	2104.2	2430.5	2831.9	3257.4	3796.8
$d_{x^2-y^2}$	6871.0	6762.7	6663.7	6553.7	6462.4	6372.8	6288.2	6141.3
d_{z^2}	7883.8	7749.9	7583.2	7401.3	7165.3	6875.9	6545.0	6228.1

Table S13. AILFT derived ligand field parameters computed at CASSCF (in parentheses) and NEVPT2 level of theory for complexes **1** and **2**. The values of *B*, *C*, ξ parameters are provided in units of cm⁻¹.

Parameter	Free Co(II)	1	2	% reduction	
ξ	527	514.6	507.1	2.353	3.776
<i>B</i>	1040.3 (1251.9)	1025.2 (1189.3)	981.9 (1167.9)	1.452 (5.000)	5.614 (6.710)
<i>C</i>	4157.7 (4621.1)	3923.6 (4412.3)	3901.4 (4373.2)	5.631 (4.518)	6.164 (5.365)
<i>C/B</i>	3.997 (3.691)	3.827 (3.710)	3.973 (3.745)	4.253 (-0.515)	0.600 (-1.463)
$\% \text{ reduction} = 1 - \left(\frac{\text{complex}}{\text{free Co(II)}} \right) \times 100$					

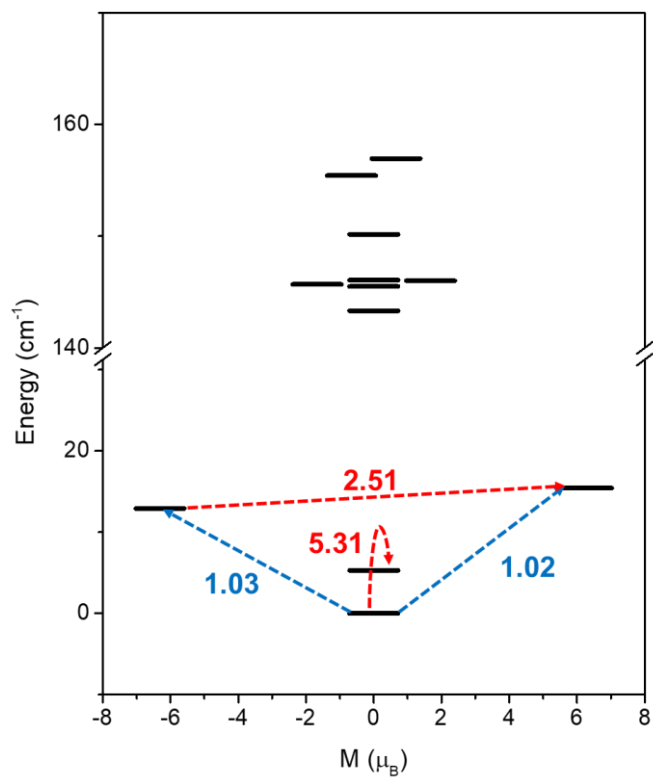


Figure S15. POLY_ANISO simulated energy spectrum of exchange coupled states in complex 1. Black bars are the energies of exchange-coupled states arranged according to the associated magnetic moments. The dotted red lines and numbers represent the possibility of quantum tunnelling between the states, while blue arrows/numbers represent the possibility of Orbach relaxations.

Table S14. BS-DFT computed energies of high-spin and broken-symmetry solution of complex **1** using $H=-2JS_1S_2$ formalism.

Solution	Energy (E _h)	ρ^{Co1}	ρ^{Co2}	$\langle S^{**2} \rangle$	J (cm ⁻¹)
HS	-7409.811455	2.6443	2.6443	12.0296	-3.72
BS1	-7409.811607	-2.6427	2.6427	3.0285	

J values are estimated using the following equation,

$$J = -\frac{E_{HS} - E_{BS}}{S_{HS}^2 - S_{BS}^2}$$

Table S15. BS-DFT computed energies of high-spin and broken-symmetry solution of complex **2** using $H=-2JS_1S_2$ formalism.

Solution	Energy (E _h)	ρ^{Co1}	ρ^{Co2}	$\langle S^{**2} \rangle$	J (cm ⁻¹)
HS	-7349.13518323578	2.643390	2.643390	12.0160	-0.00002
BS1	-7349.13518323484	-2.643390	2.643390	3.0160	

J values are estimated using the following equation,

$$J = -\frac{E_{HS} - E_{BS}}{S_{HS}^2 - S_{BS}^2}$$

Table S16. Energies of low-lying pseudo-KDs, associated g-values, and tunneling splitting for complex **1** obtained from the POLY_ANISO simulation.

Energy of Exchange doublets	g_{zz}	Δ tunneling
0.00	0.007244	5.31
5.31		
12.92	12.88903	2.52
15.44		
143.33	0.000586	2.17
145.50		
145.69	5.873261	0.32
146.01		
146.07	0.001463	4.09
150.16		
155.43	7.821624	1.52
156.94		
280.54	0.002637	0.96
281.51		
295.91	11.61671	0.07
295.99		

Table S17. RASSCF computed D , g , and E values for complexes **1** and **2** obtained from MOLCAS code.

Complex 1	Spin-free energies		Computed D values			
Energies of KDs (cm-1)		0.00	Xa	0.999212	-0.023035	0.032332
0.00	⁴ T _{1g}	724.26	Ya	0.023592	0.999578	-0.016973
139.84		1229.62	Za	-0.031928	0.017723	0.999333
g _x = 2.079795113	⁴ T _{2g}	7311.31			D =	66.4327
g _y = 3.583276885		7770.34			E =	-12.5883
g _z = 6.637110995		8468.35				
	⁴ A _{2g}	16172.42				
			Za is the orientation of the main magnetic axes			

Complex 2	Spin-free energies		Computed D values			
Energies of KDs (cm-1)	⁴ A _g	0.00	Xa	0.999771	-0.021286	0.002288
0.00	⁴ T ₂	3290.40	Ya	0.021276	0.999765	0.004200
31.68		5277.58	Za	-0.002377	-0.004151	0.999989
g _x = 2.372423777	⁴ T ₁	5566.67			D =	14.7919
g _y = 2.288276188		6918.99			E =	-3.2763
g _z = 2.175636467		8767.83				
		8950.71				
			Za is the orientation of the main magnetic axes			

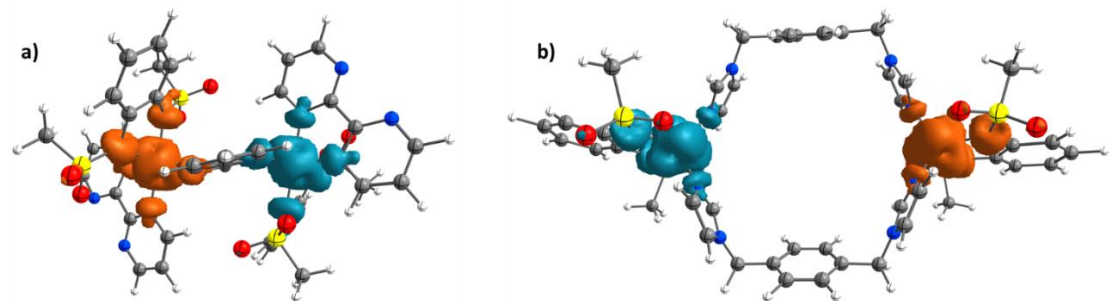


Figure S16. DFT calculated spin-density plot for the ground state ($S=0$) of complex (a) **1** and (b) **2**; the positive and negative spin densities are represented by orange and blue colour, respectively. The isodensity surface represented here corresponds to a value of $0.002 \text{ e}^-/\text{bohr}^3$.

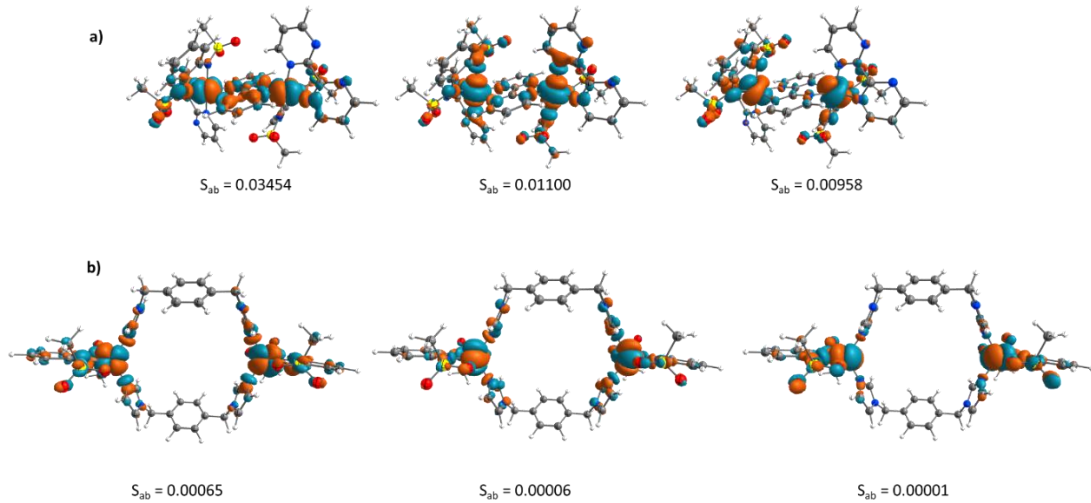


Figure S17. DFT calculated overlap integrals for complex (a) **1** and (b) **2**. The isodensity surface represented here corresponds to a value of $0.03 \text{ e}^-/\text{bohr}^3$.

Reference:

- S1) SAINT Software Users Guide, version 7.0; Bruker Analytical X-ray Systems: Madison, WI, 1999.
- S2) Sheldrick, G. M. SADABS, version 2.03; Bruker Analytical X-ray Systems: Madison, WI, 2000.
- S3) Sheldrick, G. M. SHELXTL, version 6.14; Bruker AXS, Inc.: Madison, WI, 2000–2003.
- S4) O. V. Dolomanov, L. J. Bourhis, R. J. Gildea, J. A. K. Howard, H. Puschmann, OLEX2: A Complete Structure Solution, Refinement and Analysis Program. *J. Appl. Crystallogr.* 2009, 42 (2), 339–341.
- S5) Neese, F. Software Update: The ORCA Program System, Version 4.0. *Wiley Interdiscip. Rev. Comput. Mol. Sci.* **2018**, 8, 1–6.
- S6) Neese, F.; Wennmohs, F.; Becker, U.; Ripplinger, C. The ORCA Quantum Chemistry Program Package. *J. Chem. Phys.* **2020**, 152.
- S7) Becke, A. D. Density-Functional Exchange-Energy Approximation with Correct Asymptotic Behaviour. *Phys. Rev. A* **1988**, 38, 3098–3100.
- S8) Perdew, J. P. Density-Functional Approximation for the Correlation Energy of the Inhomogeneous Electron Gas. *Phys. Rev. B* **1986**, 33, 8822–8824.
- S9) Weigend, F.; Ahlrichs, R. Balanced Basis Sets of Split Valence, Triple Zeta Valence and Quadruple Zeta Valence Quality for H to Rn: Design and Assessment of Accuracy. *Phys. Chem. Chem. Phys.* **2005**, 7, 3297–3305.
- S10) Becke, A. D. A New Mixing of Hartree-Fock and Local Density-Functional Theories. *J. Chem. Phys.* **1993**, 98, 1372–1377.
- S11) Grimme, S.; Antony, J.; Ehrlich, S.; Krieg, H. A Consistent and Accurate Ab Initio Parametrization of Density Functional Dispersion Correction (DFT-D) for the 94 Elements H-Pu. *J. Chem. Phys.* **2010**, 132.
- S12) Grimme, S.; Ehrlich, S.; Lars, G. Effect of the Damping Function in Dispersion Corrected Density Functional Theory. *J. Comput. Chem.* **2011**, 32, 1456–1465.

- S13) Ganyushin, D.; Neese, F. First-principles calculations of zerofield splitting parameters. *J. Chem. Phys.* **2006**, 125, 024103.
- S14) Hess, B. A.; Marian, C. M.; Wahlgren, U.; Gropen, O. A mean-field spin-orbit method applicable to correlated wavefunctions. *Chem. Phys. Lett.* **1996**, 251, 365–371.
- S15) Neese, F. Efficient and accurate approximations to the molecular spin-orbit coupling operator and their use in molecular g-tensor calculations. *J. Chem. Phys.* **2005**, 122, 034107.
- S16) Aquilante, F.; Autschbach, J.; Carlson, R. K.; Chibotaru, L. F.; Delcey, M. G.; De Vico, L.; Fdez. Galván, I.; Ferré, N.; Frutos, L. M.; Gagliardi, L.; et al. Molcas 8: New capabilities for multiconfigurational quantum chemical calculations across the periodic table. *J. Comput. Chem.* **2016**, 37 (5), 506.
- S17) Chibotaru, L. F.; Ungur, L. Ab initio calculation of anisotropic magnetic properties of complexes. I. Unique definition of pseudo spin Hamiltonians and their derivation *J. Chem. Phys.* **2012**, 137, 064112.
- S18) Chibotaru, L. F.; Ungur, L.; Aronica, C.; Elmoll, H.; Pilet, G.; Luneau, D. Structure, Magnetism, and Theoretical Study of a Mixed-Valence CoII3CoIII4 Heptanuclear Wheel: Lack of SMM Behavior despite Negative Magnetic Anisotropy. *J. Am. Chem. Soc.* **2008**, 130, 12445.
- S19) Soumalya, R.; Shukla, P.; Sahu, P. P.; Sun, Y.; Ahmed, N.; Sahoo, S. C.; Wang, X. Y.; Singh, S. K.; Das, S. Zero-field Slow Magnetic Relaxation Behavior of Dy²⁺ in a Series of Dinuclear Ln²⁺. (Ln=Dy, Tb, Gd and Er) Complexes: A Combined Experimental and Theoretical Study, *Eur. J. Inorg. Chem.* **2022**, e202100983.
- S20) Langley, S. K.; Ungur, L.; Chilton, N. F.; Moubaraki, B.; Chibotaru, L. F.; Murray, K. S. Single-Molecule Magnetism in a Family of {Co₂Dy^{III} 2} Butterfly Complexes: Effects of Ligand Replacement on the Dynamics of Magnetic Relaxation. *Inorg. Chem.* **2014**, 53, 4303–4315.
- S21) Kharwar, A. K.; Mondal, A.; Sarkar, A.; Rajaraman, G.; Konar, S. Modulation

- of Magnetic Anisotropy and Exchange Interaction in Phenoxide-Bridged Dinuclear Co(II) Complexes. *Inorg. Chem.* **2021**, *60* (16), 11948–11956.
- S22) Saha, S.; Das, K. S.; Sharma, T.; Bala, S.; Adhikary, A.; Huang, G.-Z.; Tong, M.-L.; Ghosh, A.; Das, B.; Rajaraman, G.; Mondal, R. Synergistic Experimental and Theoretical Studies of Luminescent–Magnetic Ln₂Zn₆ Clusters . *Inorg. Chem.* **2022**, *61* (4), 2141–2153.
- S23) Lalioti, N.; Nastopoulos, V.; Panagiotou, N.; Tasiopoulos, A.; Ioannidis, N.; van Slageren, J.; Zhang, P.; Rajaraman, G.; Swain, A.; Tangoulis, V. A Nonsymmetric Dy₂ Single-Molecule Magnet with Two Relaxation Processes Triggered by an External Magnetic Field: A Theoretical and Integrated EPR Study of the Role of Magnetic-Site Dilution . *Dalton Transactions*. **2022**, 1985–1994.
- S24) Liu, J. L.; Wu, J. Y.; Huang, G. Z.; Chen, Y. C.; Jia, J. H.; Ungur, L.; Chibotaru, L. F.; Chen, X. M.; Tong, M. L. Desolvation-Driven 100-Fold Slow-down of Tunneling Relaxation Rate in Co(II)-Dy(III) Single-Molecule Magnets through a Single-Crystal-to-Single-Crystal Process. *Sci. Rep.* **2015**, *5*, 1–9.
- S25) Yamaguchi, K.; Takahara, Y.; Fueno, T.; Houk, K. N. Extended Hartree-Fock (EHF) Theory in Chemical Reactions. *Theor. Chim. Acta* **1988**, *73*, 337–364.
- S26) Yamaguchi, K.; Fukui, H.; Fueno, T. Molecular orbital (MO) theory for magnetically interacting organic compounds. Ab-initio MO calculations of the effective exchange integrals for cyclophane-type carbene dimers. *Chem. Lett.* **1986**, No. 3, 625–628.
- S27) Izsák, R.; Neese, F. Speeding up Spin-Component-Scaled Third-Order Perturbation Theory with the Chain of Spheres Approximation : The COSX-SCS-MP3 Method. *Mol. Phys.* **2013**, *111*, 1190–1195.